Journal of Power Sources 202 (2012) 246–252

Contents lists available at SciVerse ScienceDirect

Journal of Power Sources

journal homepage: www.elsevier.com/locate/jpowsour

Single crystalline lithium titanate nanostructure with enhanced rate performance for lithium ion battery

Jun Lu, Caiyun Nan, Qing Peng, Yadong Li*

Department of Chemistry, Tsinghua University, Beijing 100084, PR China

ARTICLE INFO

Article history:
Received 17 June 2011
Received in revised form 1 November 2011
Accepted 15 November 2011
Available online 9 December 2011

Keywords:
Lithium titanate oxide
Single crystalline
Low-temperature transformation

ABSTRACT

Here we report the synthesis and electrochemical performance of 40 nm near-uniform lithium titanate ($Li_4Ti_5O_{12}$) single crystals. The cubic spinel $Li_4Ti_5O_{12}$ nanocrystals are transformed without size changes at 400 °C from cubic NaCl type $(Li_{0.4}H_{0.6})_2TiO_3$ nanocrystals that are prepared from hydrothermal synthesized α-Li_2TiO_3. The prepared $Li_4Ti_5O_{12}$ nanocrystals show reduced charge-transfer impedance and exhibit favorable performance under high current charging/discharging due to the reduced Li^+ ion diffusion path.

1. Introduction

Secondary lithium ion batteries (LIBs) have been of great potential for applications in the hybrid electric vehicles (HEVs) and electric vehicles (EVs), due to the unique features such as high energy density and efficiency, long cycling life and environmental friendliness [1–3]. The key challenges for LIBs have been the insufficient power density and safety issues which are aroused from the intrinsic low conductivities of materials and the side reactions with the electrolytes under extreme operation conditions, respectively [4–8]. To solve these problems, nanostructured forms of materials with stable structure and inert reactivity to electrolytes have attracted tremendous attention, because these nanomaterials have shown excellent rate capability as well as safety due to the reduced diffusion time for Li^+ ions and surface current density in terms of $\tau \propto 1/R^2$ and $i \propto R$, respectively [9–11]. Nanostructured spinel $Li_4Ti_5O_{12}$ is one of the examples which have been regarded as potential candidate for anode materials in power LIBs [12–17].

The outstanding features of $Li_4Ti_5O_{12}$ nanostructure can be summarized as follows: (1) the zero-strain structure in which the insertion/desertion of Li^+ ions occur on tetrahedral 8a and octahedral 16c sites with tiny lattice change [18–22]; (2) the potential based on Ti^{3+}/Ti^{4+} redox couple is 1.5 V verse Li metal, so high that no reduction of organic electrolytes into surface electrolyte interface (SEI) could occur, and Li dendrites are unlikely to form even when over discharged [23,24]; (3) the Li^+ insertion/desertion reactions are highly reversible compared to graphite and alloys, ensure this material with high columbic efficiency and long cycling life [15]; (4) nanostructures of $Li_4Ti_5O_{12}$ show favorable rate capability as the Li^+ diffusion path becomes short and the surface contact area is large [2,5,8]. These features make $Li_4Ti_5O_{12}$ nanomaterials the ideal candidate for anode in high power LIBs, even though the 175 mAh g^{-1} specific capacity is not in favor of this spinel material. Recently, efforts have been made to the synthesis and electrochemical investigation of nanostructured $Li_4Ti_5O_{12}$ materials, including 1D nanorods [25,26], 2D nanosheets [27], hollow spheres [28,29] and assembled microspheres [30].

While the perspective of nanostructured $Li_4Ti_5O_{12}$ is fascinating, the synthesis of $Li_4Ti_5O_{12}$ nanomaterials with uniform morphology and single crystalline nanostructure has been a challenge. The reason for the difficulty may be this: sintering of the material accompanying the essential high-temperature calcinations (500–1000 °C) in conventional approaches would destruct the morphologies of the nanostructures and result into wide size-distributed materials [31–33]. The most effective solution to the sintering is to prepare $Li_4Ti_5O_{12}$ nanostructure at the convenient temperature low enough to prevent the sintering. As a result, convenient low-temperature approaches for uniform single crystalline $Li_4Ti_5O_{12}$ nanostructure would be of importance for the application of this spinel material in high power LIBs.

In this effort, we propose a low-temperature strategy for near-uniform $Li_4Ti_5O_{12}$ single crystals with 40 nm in size. By taking advantage of metastable cubic $(Li_{0.4}H_{0.6})_2TiO_3$ nanocrystals delithiated from α-Li_2TiO_3 as the intermediate, well dispersed crystalline $Li_4Ti_5O_{12}$ nanocrystals are obtained at 400 °C for 2 h. The as-synthesized sample nanocrystals are phase pure cubic spinel

* Corresponding author. Tel.: +86 10 62772350; fax: +86 10 62788765.
E-mail address: ydli@mail.tsinghua.edu.cn (Y. Li).

0378-7753/$ – see front matter © 2011 Elsevier B.V. All rights reserved.
doi:10.1016/j.jpowsour.2011.11.032

$Li_4Ti_5O_{12}$. It has been clear that the sizes, surface areas and morphologies of the samples before and after the calcination treatment are in well accordance by various characterizations, indicating the calcination at 400 °C is sintering-resistant. Impedance spectroscopy (EIS) and galvanostatic tests indicate that the 40 nm single crystalline $Li_4Ti_5O_{12}$ nanomaterials exhibit reduced charge-transfer impedance and enhanced rate performance comparing with the reference sample synthesized at 700 °C.

2. Experimental

2.1. Synthesis of $Li_4Ti_5O_{12}$ nanostructure

The reagents were purchased from China National Medicines Corp., Ltd. Hydrothermal method similar with Ref. [34] has been applied to synthesize α-Li_2TiO_3, using 4.5 nm anatase TiO_2 prepared using the method in Ref. [35]. 0.5 g as-prepared anatase TiO_2 was added into 2 M, 40 mL LiOH aqueous solution under vigorous stirring. The mixture was transferred into a Teflon-lined autoclave, and then maintained at 160 °C for 48 h. The precipitate collected from the bottom of the auto-clave by centrifugation was white-colored α-Li_2TiO_3, with a much larger Li/Ti mole ratio than 0.8 for $Li_4Ti_5O_{12}$. To prepare $(Li_{0.4}H_{0.6})_2TiO_3$, approximately 10 mL, 1 M HCl aqueous solution was applied to exchange excess Li^+ ions to make the Li/Ti ratio 0.8. After washing, the product was further centrifuged and dried in the 70 °C oven. The calcinations of product were carried out at 400 °C for 2 h in which nanosized $Li_4Ti_5O_{12}$ was obtained. In addition, reference sample was prepared from the product at 700 °C for 2 h.

2.2. Characterizations

The powder X-ray diffraction patterns of $Li_{0.8}H_{1.2}TiO_3$ and $Li_4Ti_5O_{12}$ synthesized at 400 °C and 700 °C were collected on Rikagu D/max 2500 with Cu Kα radiation (λ = 0.154056 nm). The sizes and morphologies of $(Li_{0.4}H_{0.6})_2TiO_3$ and $Li_4Ti_5O_{12}$ synthesized at 400 °C were characterized by TEM (JEOL JSM-6301F at 100 kV), FESEM (LEO-1530) and HRTEM (FEI Tecnai G2 F20 S-Twin working at 200 kV). The thermal gravity curve of $(Li_{0.4}H_{0.6})_2TiO_3$ was recorded on TGA 2050 from room temperature to 800 °C at a heating rate of 15 °C min^{-1} under air flow. The FT-IR spectra of $(Li_{0.4}H_{0.6})_2TiO_3$ were collected on Perkin-Elmer Spectrum GX. The specific surface area of $(Li_{0.4}H_{0.6})_2TiO_3$ and 400 °C prepared $Li_4Ti_5O_{12}$ were measured by BET method using Quantachrome, Autosorb-1. Also, X-ray photoelectron spectroscopy (XPS) characterization was carried out on PHI-5300 to determine the valance of Ti element in $(Li_{0.4}H_{0.6})_2TiO_3$.

2.3. Electrochemical tests

CR2016 coin-type cells were employed to characterize the electrochemical properties of nanostructured and reference $Li_4Ti_5O_{12}$. Blends of active material, acetylene black and PTFE in the mass ratio of 8:1:1 were fully grounded and then pasted on copper foil with ~3.5 mg cm^{-2} loading density. Then the loaded copper foil was dried in a 120 °C vacuum oven for 12 h. Coin-type cells were fabricated in an Ar-filled glove box using lithium metal as the counter electrode, celgard 2300 membrane as the separator and 1 M $LiPF_6$ solution in DMC/EC (1:1 in volume) as the electrolyte. The rate and cycling examinations were carried out on battery testing system (BTS-5V 5 mA, Neware) at a voltage range of 2.5–0.9 V. The electrochemical impedance spectroscopy (EIS) measurement was carried out on CHI 660D electrochemical station with the frequency range of 10 kHz to 0.1 Hz and RMS potential of 10 mV.

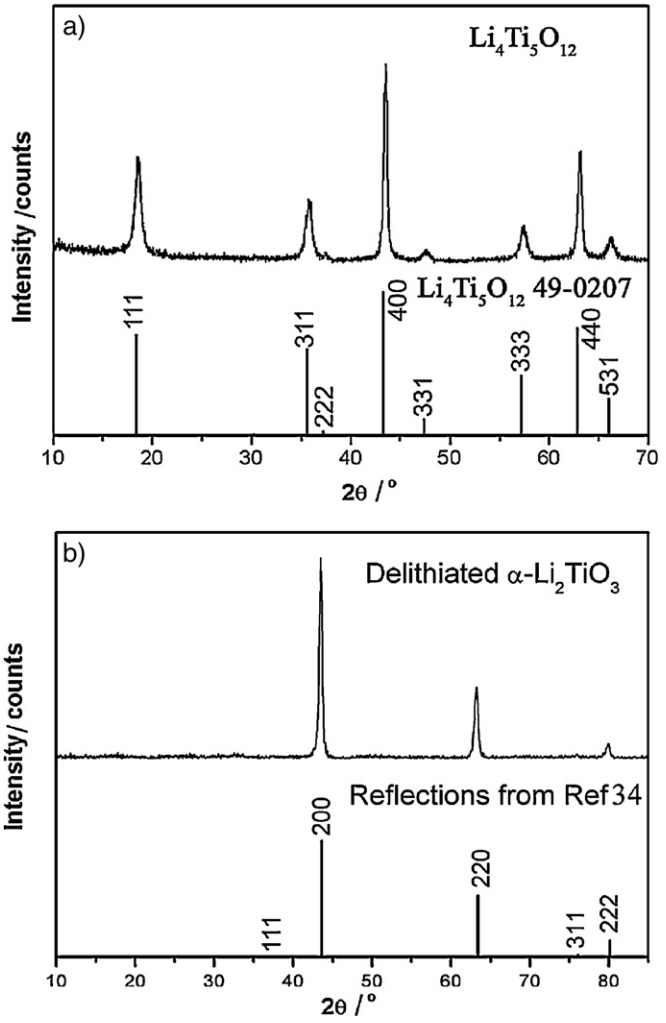

Fig. 1. XRD pattern for $Li_4Ti_5O_{12}$ single crystalline nanoparticles (a) and delithiated α-Li_2TiO_3 nanocrystals (b).

3. Results and discussion

3.1. Structural and morphology characterizations

Fig. 1 shows the XRD patterns of as-synthesized sample after and before 400 °C treatment. The diffraction pattern of calcination product, $Li_4Ti_5O_{12}$ is shown in Fig. 1a. The pattern is identical with the standard $Li_4Ti_5O_{12}$ (JCPDS File No. 49-0207), which confirms spinel structure of product. No peaks of impurities such as TiO_2, α- or γ-Li_2TiO_3 are found in the pattern, indicating the transformation though the calcinations temperature was completed at 400 °C. The diffraction pattern of delithiated α-Li_2TiO_3 nanocrystals in Fig. 1b is identical with the cubic NaCl type α-Li_2TiO_3 with Li^+ and Ti^{4+} cation disorder which has been reported in Refs. [34,36]. The peaks and corresponding *d*-spacings that are $2\theta = 43.52°$ with $d = 2.079$ Å, 63.27° with 1.469 Å and 79.94° with 1.199 Å, respectively, could be indexed as (2 0 0), (2 2 0) and (2 2 2) according to the previous result of synchrotron measurements. As the delithiated forms of α-Li_2TiO_3 whose formula could be expressed as $(Li_{1-x}H_x)_2TiO_3$ are almost identical by XRD, further characterizations are carried out to determine the exact formula of the delithiated α-Li_2TiO_3.

The TGA curve in Fig. 2a shows the only weight-loss region locates at 20–400 °C with weight loss of 10.2 wt.%, indicating that the hypothetical formula of delithiated α-Li_2TiO_3 could be $(Li_{0.4}H_{0.6})_2TiO_3$ whose theoretical weight loss is 10.5 wt.%. It is

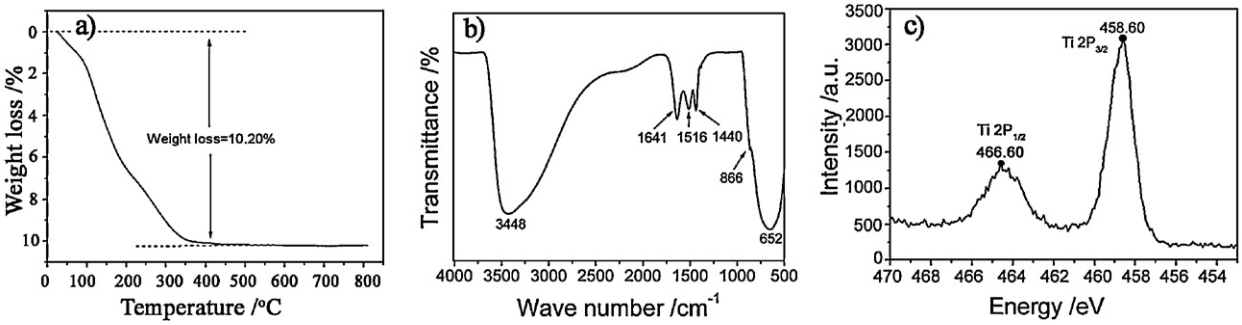

Fig. 2. TGA curve (a), FT-IR spectra (b) and XPS spectra (c) of $(Li_{0.4}H_{0.6})_2TiO_3$.

worthy noting that the Li/Ti mole ratio of $(Li_{0.4}H_{0.6})_2TiO_3$ is 0.8, exactly the Li/Ti mole ratio in $Li_4Ti_5O_{12}$ product, confirming that the hypothetical formula is rational, and that the Li^+ ions in metastable α-Li_2TiO_3 could be ion-exchanged and exactly tuned by HCl, in consistent with the previous work [34,37]. Notably, the flat plateau beyond 400 °C suggests that the transformation toward $Li_4Ti_5O_{12}$ completes at 400 °C which is confirmed in the XRD pattern of the 400 °C product. In the FT-IR spectra in Fig. 2b, wide, strong peak at 3700–2500 cm^{-1} (hydrogen-bonded O—H stretching) indicates the existence of O—H bonds in the structure which is in consistent with the hypothetical formula [36–38]. The 1516, 1440 and 866 cm^{-1} peaks could be assigned to CO_3^{2-} species, for $(Li_{0.4}H_{0.6})_2TiO_3$ would react with H_2O and CO_2 to yield Li_2CO_3 when exposing to the atmosphere, which has been reported previously [34,36]. And the final peak at 652 cm^{-1} could be the absorption of stretching Ti—O bond. From XPS plot of delithiated α-Li_2TiO_3 in Fig. 2b, the peaks of Ti $2P_{3/2}$ and $2P_{1/2}$ locate at 458.6 and 464.6 eV, respectively, indicating +4 chemical valance of Ti element, which is in consistent with chemical formula and the literature [39,40].

The morphologies and sizes of delithiated α-Li_2TiO_3 and $Li_4Ti_5O_{12}$ nanocrystals are characterized by TEM and SEM. In TEM image for α-Li_2TiO_3 (Fig. 3a), the crystal size is around 40 nm with smooth surface and near-cubic shape with narrow size distribution. Seen from Fig. 3b, the $Li_4Ti_5O_{12}$ nanostructure are cubic-like in shape and 40 nm in size. The size of the spinel material is relatively uniform, and boundaries between the $Li_4Ti_5O_{12}$ nanocrystals are clear, indicating a narrow size distribution of the nanocrystals. The morphologies, sizes and size distributions for α-Li_2TiO_3 and $Li_4Ti_5O_{12}$ samples are similar from the TEM characterizations, showing that the calcination operates without aggregation of the delithiated α-Li_2TiO_3. The SEM images further confirm the similarity between two nanocrystals. In both SEM images (Fig. 3c and d), cubic-like nanocrystals are near-uniform and well dispersed.

To get information of the specific surface area change caused by the calcination process, BET analysis is carried out for delithiated α-Li_2TiO_3 and $Li_4Ti_5O_{12}$ nanocrystals. The measured specific surface areas for delithiated α-Li_2TiO_3 and $Li_4Ti_5O_{12}$ materials are 45.7 and 43.7 $m^2\,g^{-1}$, respectively. The average size for $Li_4Ti_5O_{12}$ calculated from the BET surface area by the equation $S = 6/\rho R$ is 39 nm, which is in well agreement with the observation in the TEM image (Fig. 3b). The preserved surface area is another piece of evidence that the low-temperature calcination process is sintering-resistant.

HRTEM and selected area electron diffraction (SAED) images for both samples are present in Fig. 4a–d. The HRTEM image for delithiated α-Li_2TiO_3 crystals (Fig. 4a) shows a size ranges from 30 to 50 nm, and the exact shape becomes sphere-like. The *d*-spacings in SAED of delithiated α-Li_2TiO_3 in Fig. 4b are 2.40, 2.08 and 1.49 Å, respectively, matching the *d*-spacings of (1 1 1), (2 0 0) and (0 2 2) facets of α-Li_2TiO_3 reflections in Ref. [34]. These observed lattice spacings have also been compared with that of spinel $Li_4Ti_5O_{12}$ considering that the metastable α-Li_2TiO_3 would transform to $Li_4Ti_5O_{12}$ under the electron beam of HRTEM, and no rational match with spinel $Li_4Ti_5O_{12}$ was found. For $Li_4Ti_5O_{12}$ (Fig. 4c and d), the nanostructure indicates the product $Li_4Ti_5O_{12}$ is well crystalline with clear lattice fringes and smooth surface, and the discernable vacancies in the particle could be the result of the release of H_2O during calcination. Indexed diffraction pattern confirms the single crystalline structure, as only one series of diffraction pattern is present.

As a conclusion of characterizations, single crystalline $Li_4Ti_5O_{12}$ nanostructure with a narrow size distribution and well dispersion is obtained, and the method is sinter-resistant as well as convenient. The scheme for our strategy is present in Scheme 1. The transformation of delithiated cubic NaCl-type α-Li_2TiO_3 to cubic spinel $Li_4Ti_5O_{12}$ is carried out at the calcination temperature of 400 °C, which is lower than the temperature (500–1000 °C) applied in other literature. The low-temperature transformation of α-Li_2TiO_3 to $Li_4Ti_5O_{12}$ nanocrystals could be relevant with the thermodynamic and structural properties of metastable $(Li_{0.4}H_{0.6})_2TiO_3$. The structural metastability of $(Li_{0.4}H_{0.6})_2TiO_3$ reduces Gibbs free energy change for total reaction, and the structural similarity of cubic $(Li_{0.4}H_{0.6})_2TiO_3$ and cubic $Li_4Ti_5O_{12}$ reduces activated energy for cation rearrangement during the structural changes, comparing with the traditional transformation from rutile or anatase TiO_2 and lithium salt to $Li_4Ti_5O_{12}$ [36]. Besides, that atom-scale blending of Li^+ and Ti^{4+} ions in the $(Li_{0.4}H_{0.6})_2TiO_3$ structure would shorten the time needed for transformation completion in terms of improved reaction rate, since the rate of solid-state reaction and the mixing state of precursor are positively related.

3.2. Application of $Li_4Ti_5O_{12}$ single nanocrystals in Li-ion battery

The electrochemical tests of spinel $Li_4Ti_5O_{12}$ nanostructure and reference sample are carried out by galvanostatic methods. It should be noted that the reference sample with spinel $Li_4Ti_5O_{12}$ pure phase and a BET surface area of 22.2 $m^2\,g^{-1}$ is prepared with the identical delithiated α-Li_2TiO_3 precursor at 700 °C for 2 h (XRD, SEM are available in supporting information), and consists of microparticle together with nanoparticles. Figs. 5 and 6 present the rate performances and the discharge curves of single crystalline

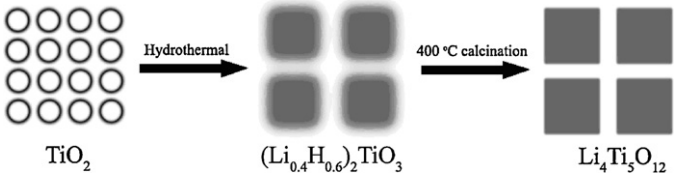

Scheme 1. Two-step route for spinel $Li_4Ti_5O_{12}$ single crystals with morphology preservation.

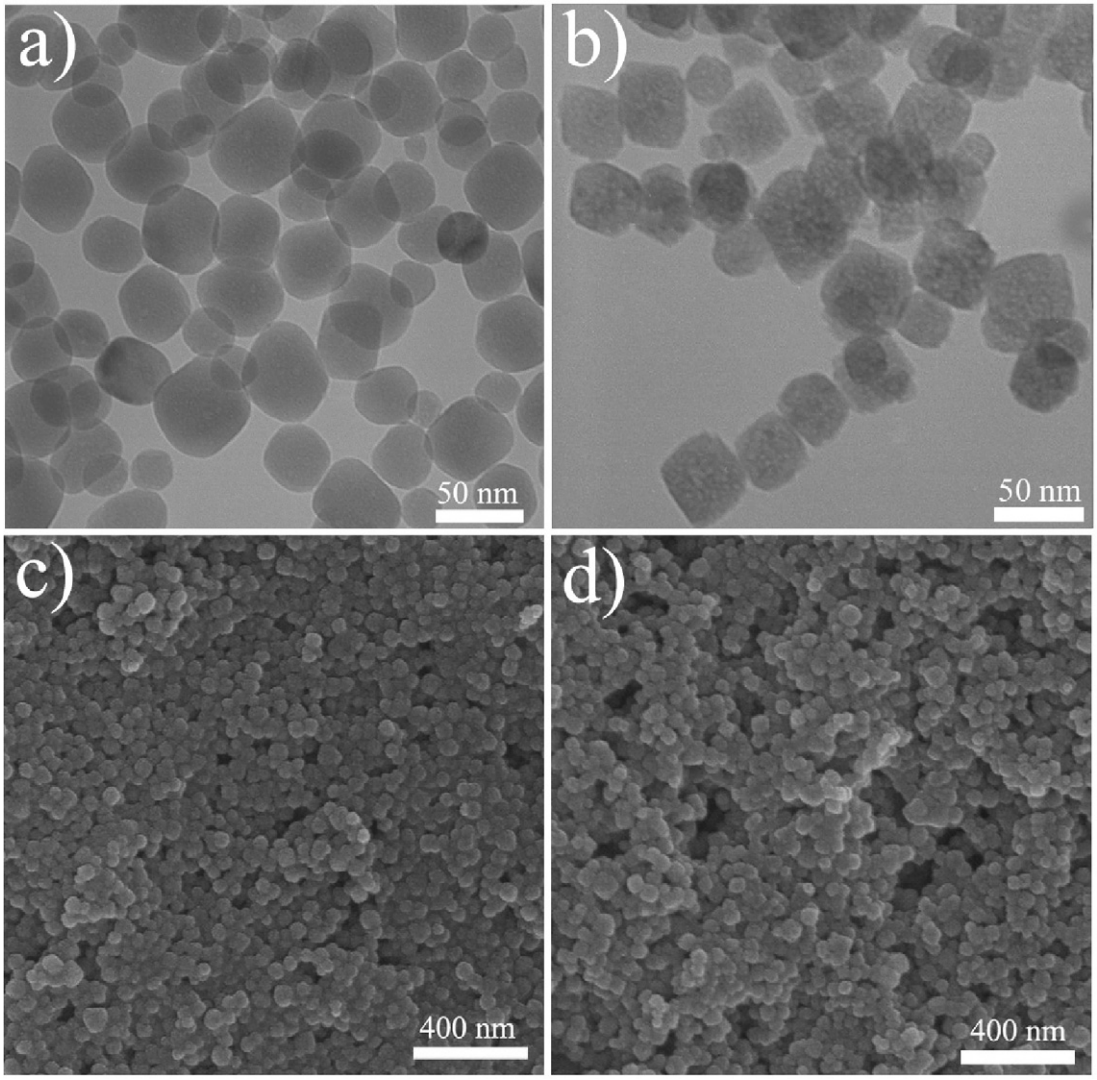

Fig. 3. TEM and SEM images for $(Li_{0.4}H_{0.6})_2TiO_3$ nanocrystals (a, c) and $Li_4Ti_5O_{12}$ single crystals (b, d).

$Li_4Ti_5O_{12}$ and reference sample cycled from 0.5 C to 5 C for 10 times each. In Fig. 5, the segments for the $Li_4Ti_5O_{12}$ nanocrystals at different rates are flat, and the discharge–charge plots almost overlap for all cycles except the first one, indicating the well cycling performance as well as the good columbic efficiency of the $Li_4Ti_5O_{12}$ material. The initial and second discharge capacities of nanostructured sample at 0.5 C are 184 mAh g^{-1} and 175 mAh g^{-1}, and the discharge/charge capacity for 0.5 C retained an accessible capacity of 172 mAh g^{-1} with well reversibility. For the reference sample, 173 and 165 mAh g^{-1} are the initial and second discharge capacities, and 162 mAh g^{-1} is the average capacity for the rest cycles of the 0.5 C step. When the current rate increases, the nanostructured sample delivers 165, 159, 156, 150 and 140 mAh g^{-1} at 1, 2, 3, 4 and 5 C, respectively, with well stability and reversibility. To the reference sample, low rate capability and cycling instability are found as the capacity decrease toward increased rate is serious. When the two samples get back to 1 C cycling after 5 C, the high capacities and well cycling properties are retained, showing the cycling stability of $Li_4Ti_5O_{12}$. The compare on rate capabilities of spinel $Li_4Ti_5O_{12}$ nanostructure and reference shows that the near-uniform nanomaterial has a larger capacity as well as better cycling stability under higher rates.

For close inspections, the final discharge curves of samples for every rate step are present in Fig. 6. It is found that the voltage plateaus for the two-phase reaction are about 1.5 V. Meanwhile, the voltage plateau and specific capacities for both samples drop when the rate increases due to the electric resistance. The voltage plateaus for $Li_4Ti_5O_{12}$ single crystals last longer than those of the reference sample, while the voltage drops for the single crystals caused by the polarization are close to the reference sample. As mentioned above, the 400 °C calcinated sample has a large specific surface area and reduced Li^+ ion diffusion path. What we find from the compare of discharge curves is that electrical resistances for both samples are similar, while the percentage of $Li_4Ti_5O_{12}$ participating in the charging/discharging process increases for the nanosized sample because nanosized $Li_4Ti_5O_{12}$ material makes Li^+ easier to insert/desert from the material. This observation indicates that the improved capacity of $Li_4Ti_5O_{12}$ nanomaterial under high charging/discharging process is more relevant with the nanosized Li^+ ion diffusion path of the nanostructure rather than reduced polarization. Also, the single crystalline structure of $Li_4Ti_5O_{12}$ nanocrystals could also help to make Li^+ ions easier to come through the material, because no crystal boundaries would block the diffusion path in the single crystals of $Li_4Ti_5O_{12}$ and $Li_7Ti_5O_{12}$ during the charging/discharging process. Further experiments shall be carried out so as to understand the impact of single crystalline structure on the electrochemical properties.

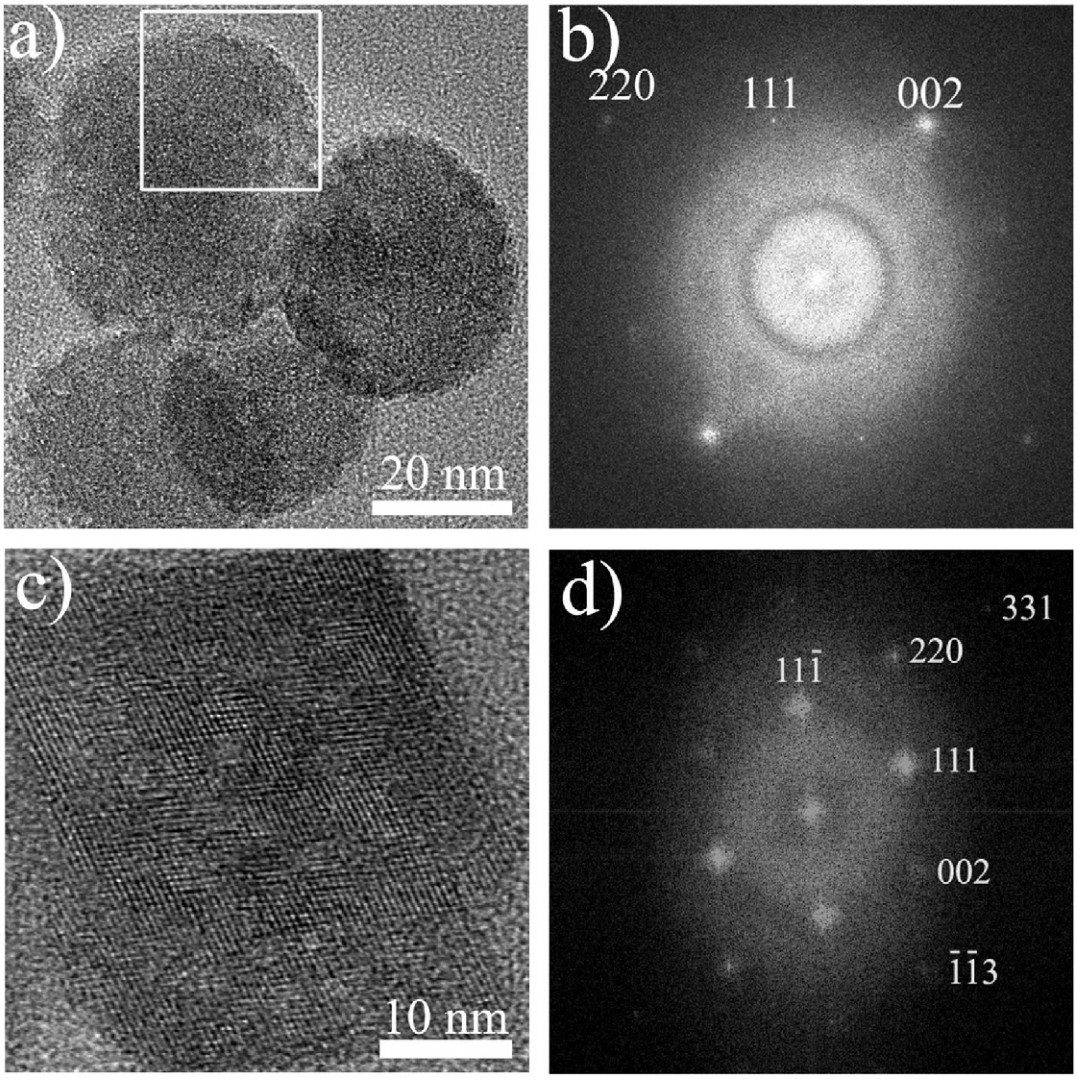

Fig. 4. HRTEM image and SAED pattern for $(Li_{0.4}H_{0.6})_2TiO_3$, the inset box is selected area for electron diffraction (a, b); HRTEM image and SAED for $Li_4Ti_5O_{12}$ single crystals (c, d).

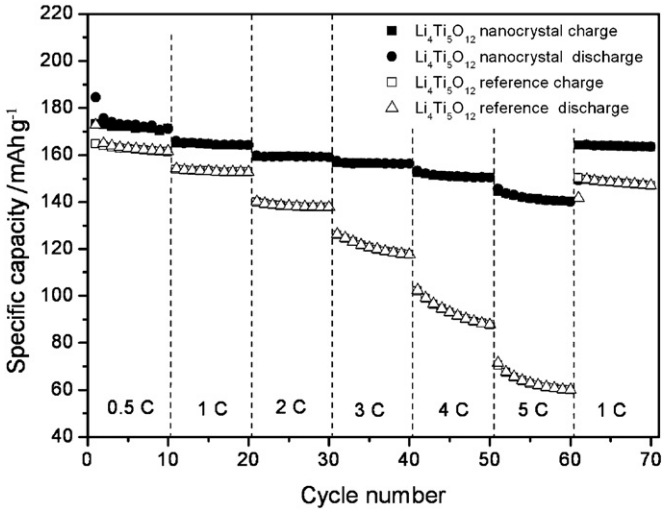

Fig. 5. Cycling performances for the nanostructured and reference $Li_4Ti_5O_{12}$. Filled dots are for nanocrystals, and hollow dots are for reference sample. Both batteries are cycled from 0.5 C to 5 C and then to 1 C, each for 10 circles.

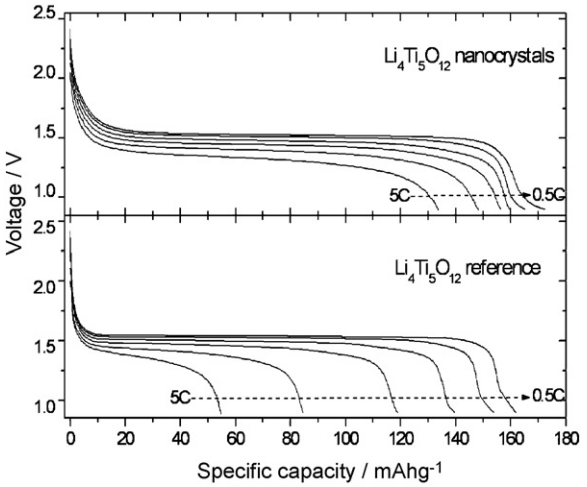

Fig. 6. Discharge curves for the nanocrystalline and reference samples. Charge/discharge rates range from 0.5, 1, 2, 3, 4 to 5 C for both materials.

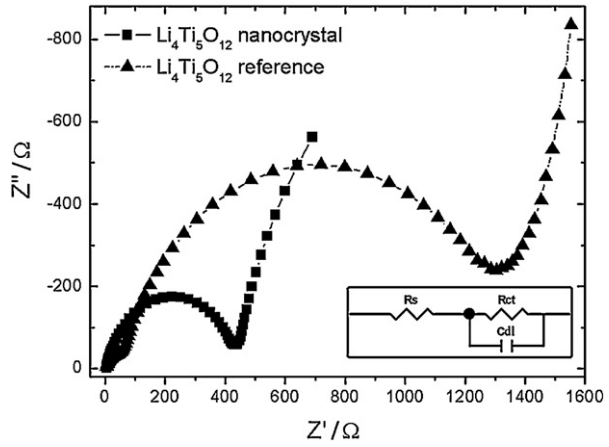

Fig. 7. Nyquist plots for the nanocrystalline and reference samples. R_s, R_{ct} and C_{dl} of the equivalent circuit in the inset represent the electrolyte resistance, charge-transfer resistance for both Li^+ ions and electrons, and double layer capacitance, respectively.

Table 1
Simulated value for R_s, R_{ct}, and C_{dl} parameters of the nanocrystals and reference sample.

	R_s (Ω)	R_{ct} (Ω)	C_{dl} (F)
Nanocrystals	4.5	441	5.2E−6
Reference sample	3.8	1453	7.4E−6

To explorer the relevance of electrochemical impedances with the nanostructured and microsized materials, electronic impedance spectroscopy (EIS) measurements are carried out for nanostructured and reference samples before galvanostatic tests. Fig. 7 shows the EIS curves in Nyquist plot and equivalent circuit for the samples. For both samples, similar semicircles at the high-to-medium frequency region and sloping lines at low frequency region indicate that the electrochemical mechanism for two samples are identical, and are consistent with the Randles electroinsertion mechanism. The semicircle corresponding to the interfacial electrochemical reactions is mainly relevant with the charge-transfer resistance, and the sloping lines at low frequency shows the Li^+ ion diffusion in the solid-state electrode material. Slight depressions for both semicircles indicate that the active materials for electrodes are sub-microsized, which is in consistent with TEM and SEM observations of $Li_4Ti_5O_{12}$ nanocrystals and the reference material [41]. Considering the impedances aroused from the electrolyte and charge-transfer process, R_s and R_{ct} are calculated from the equivalent circuit and listed in Table 1. From the table, it shows that the single crystalline $Li_4Ti_5O_{12}$ nanomaterial exhibits similar R_s and much reduced R_{ct} to those of reference $Li_4Ti_5O_{12}$. The larger BET surface area of the spinel nanocrystals could be the reason for the small R_{ct} parameter, which makes the charge transfer on the interface of spinel material and electrolyte easy and further helps to promote the rate performance.

4. Conclusions

In summary, we propose a convenient strategy for $Li_4Ti_5O_{12}$ spinel nanomaterial as the anode for LIBs with profound rate capability. By various characterizations, it has been proved that, the strategy that applies delithiated metastable α-Li_2TiO_3 nanocrystals as the precursor has not only turned $Li_4Ti_5O_{12}$ into 40 nm single crystalline nanomaterials but also preserved the size, surface area and morphology of the precursor by reducing the time and temperature for annealing. $Li_4Ti_5O_{12}$ nanomaterial with reduced charge-transfer impedance delivers profound rate and cycling capability, showing its potential for application in high power LIBs. Furthermore, it is indicated that the improved capacity and reduced R_{ct} of the $Li_4Ti_5O_{12}$ nanomaterial can be attributed to nanosized distance for Li^+ ion diffusion in single nanocrystals and large surface area, respectively.

Acknowledgements

This work was supported by the State Key Project of Fundamental Research for Nanoscience and Nanotechnology (2011CB932401) and the Foundation for Innovative Research Groups of the National Natural Science Foundation of China (Grant No. 20921001).

Appendix A. Supplementary data

Supplementary data associated with this article can be found, in the online version, at doi:10.1016/j.jpowsour.2011.11.032.

References

[1] J.M. Tarascon, M. Armand, Nature 414 (2001) 359.
[2] P.G. Bruce, B. Scrosati, J.M. Tarascon, Angew. Chem. Int. Ed. 47 (2008) 2930.
[3] M.S. Whittingham, Chem. Rev. 104 (2004) 4271.
[4] N. Jansen, A.J. Kahaian, K.D. Kepler, P.A. Nelson, K. Amine, D.W. Dees, D.R. Vissers, M.M. Thackeray, J. Power Sources 81–82 (1999) 902.
[5] J.B. Goodenough, Y. Kim, Chem. Mater. 22 (2010) 578.
[6] Y.H. Rho, K. Kanamura, J. Solid State Chem. 177 (2004) 2094.
[7] M. Venkateswarlu, C.H. Chen, J.S. Do, C.W. Lin, T.C. Chou, B.J. Hwang, J. Power Sources 146 (2005) 204.
[8] Y.G. Guo, J.S. Hu, L.J. Wan, Adv. Mater. 20 (2008) 2878.
[9] J. Chen, F.Y. Cheng, Acc. Chem. Res. 42 (2009) 713.
[10] F.Y. Cheng, J.Z. Zhao, W. Song, C.S. Li, H. Ma, J. Chen, P.W. Shen, Inorg. Chem. 45 (2006) 2038.
[11] X.L. Xiao, L. Wang, D.S. Wang, X.M. He, Q. Peng, Y.D. Li, Nano Res. 2 (2009) 923.
[12] K. Amine, I. Belharouak, Z.H. Chen, T. Tran, H. Yumoto, N. Ota, S.T. Myung, Y.K. Sun, Adv. Mater. 22 (2010) 3052.
[13] W.J.H. Borghols, M. Wagemaker, M.U. Lafont, E.M. Kelder, F.M. Mulder, J. Am. Chem. Soc. 131 (2009) 17786.
[14] S. Prakash, P. Manikandan, K. Ramesha, M. Sathiya, J.M. Tarascon, A.K. Shukla, Chem. Mater. 22 (2010) 2857.
[15] H. Jiang, E. Hosono, M. Ichihara, I. Honma, H.S. Zhou, J. Electrochem. Soc. 155 (2008) A553.
[16] T. Ohzuku, A. Ueda, N.J. Yamamoto, J. Electrochem. Soc. 142 (1995) 1431.
[17] T.F. Yi, L.J. Jiang, J. Shu, C.B. Yue, R.S. Zhu, H.B. Qiao, J. Phys. Chem. Solids 71 (2010) 1236.
[18] M.M. Thackeray, J. Electrochem. Soc. 142 (1995) 2558.
[19] S. Schamer, W. Weppner, P. Schmid-Beurmann, J. Electrochem. Soc. 146 (1999) 857.
[20] P.P. Prosinni, R. Mancini, L. Petrucci, Solid State Ionics 144 (2001) 185.
[21] D.W. Murphy, M. Greenblatt, S.M. Zahurak, R.J. Cava, J.V. Waszczak, W.G. Hull, R.S. Hutton, Chim. Miner. 19 (1982) 441.
[22] S. Arico, P.G. Bruce, B. Scrosati, J.M. Tarascon, W.V. Schalkwijik, Nat. Mater. 4 (2005) 366.
[23] M. Wagemaker, D.R. Simon, E.M. Kelder, J. Schoonman, C. Ringpfeil, U. Haake, D. Lutzenkirchen-Hecht, R. Frahm, F.M. Mulder, Adv. Mater. 18 (2006) 3169.
[24] L. Kavan, M. Gratzel, Electrochem. Solid State Lett. 5 (2002) A39.
[25] J.R. Li, Z.L. Tang, Z.T. Zhang, Electrochem. Commun. 7 (2005) 894.
[26] Y. Li, G.L. Pan, J.W. Liu, X.P. Gao, J. Electrochem. Soc. 156 (2009) A495.
[27] J.Z. Chen, L. Yang, S.H. Fang, Y.F. Tang, Electrochem. Acta 55 (2010) 6596.
[28] C.H. Jiang, Y. Zhou, I. Honnma, T. Kudo, H.S. Zhou, J. Power Sources 166 (2007) 514.
[29] C.Y. Lin, J.G. Duh, J. Alloys Compd. 509 (2011) 3680.
[30] L.F. Shen, C.Z. Yuan, H.J. Luo, X.G. Zhang, K. Xu, Y.Y. Xia, J. Mater. Chem. 20 (2010) 6998.
[31] C.H. Jiang, M. Ichihara, I. Honnma, H.S. Zhou, Electrochem. Acta 52 (2007) 6470.
[32] A.S. Prakash, P. Manikandan, K. Ramesha, M. Sathiya, J.M. Tarascon, A.K. Shukla, Chem. Mater. 22 (2010) 2857.
[33] J. Lim, E. Choi, V. Mathew, D. Kim, D. Ahn, G. Gim, S.H. Kang, J. Kim, J. Electrochem. Soc. 158 (2011) A275.
[34] A. Laumann, K.T. Fehr, M. Wachsmann, M. Holzapfel, B.B. Iversen, Solid State Ionics 181 (2010) 1525.
[35] C. Wang, Z.X. Deng, R.D. Li, Inorg. Chem. 40 (2001) 5120.

[36] D. Fattakhova, V. Petrykin, J. Brus, T. Kostlánová, J. Dědeček, P. Krtil, Solid State Ionics 176 (2005) 1877.
[37] V.M. Zainullina, V.P. Zhukov, T.A. Denisova, L.G. Maksimova, J. Struct. Chem. 44 (2003) 180.
[38] K. Nakamoto, Infrared and Raman Spectra of Inorganic and Coordination Compounds, sixth ed., Wiley, New Jersey, 2009.
[39] C.H. Jiang, E. Hosono, M. Ichihara, I. Honnma, H.S. Zhou, J. Electrochem. Soc. 155 (2008) A553.
[40] G.E. Muilenherg, Handbook of X-ray Photoelectron Spectroscopy, Perkin-Elmer Corporation, 1979.
[41] R. Dedryvere, D. Foix, S. Franger, S. Patoux, L. Daniel, D. Gonbeau, J. Phys. Chem. C 114 (2010) 10999.